Frick, D. A., Schuessler, J. A., Sommer, M., von Blanckenburg, F. (2019): Laser Ablation In Situ Silicon Stable Isotope Analysis of Phytoliths. - *Geostandards and Geoanalytical Research*, *43*, 1, pp. 77—91.

DOI: http://doi.org/10.1111/ggr.12243

Laser ablation *in situ* silicon stable isotope analysis of phytoliths

Daniel A. Frick[1, ‡], Jan A. Schuessler[1,*], Michael Sommer[2,3], Friedhelm von Blanckenburg[1,4]

[1] GFZ German Research Centre for Geosciences, Earth Surface Geochemistry, Potsdam, Germany.

[2] Leibniz-Centre for Agricultural Landscape Research (ZALF) e. V., Working Group Si Biogeochemistry, 15374 Müncheberg, Germany.

[3] University of Potsdam, Institute of Earth and Environmental Sciences, Karl-Liebknecht-Str. 24-24, 14476 Potsdam, Germany.

[4] Institute of Geological Science, Freie Universität Berlin, Berlin.

* present address: Thermo Fisher Scientific GmbH, 28199 Bremen, Germany

‡ dfrick@gfz-potsdam.de, +49 331 288 28963

Abstract

Silicon is a beneficial element for many plants, and is deposited in plant tissue as amorphous bio-opal called phytoliths. The biochemical processes of silicon uptake and precipitation induce isotope fractionation: the mass-dependent shift in the relative abundances of the stable isotopes of silicon. At the bulk scale, δ^{30}Si ratios span from -2 to +6 ‰. To further constrain these variations *in situ,* at the scale of individual phytolith fragments, we used femtosecond laser ablation multicollector inductively coupled plasma mass spectrometry (fsLA-MC-ICP-MS).

A variety of phytoliths from grasses, trees and ferns were prepared from plant tissue or extracted from soil. Good agreement between phytolith δ^{30}Si ratios obtained by bulk solution MC-ICP-MS analysis and *in situ* isotope ratios from fsLA-MC-ICP-MS validates the method. Bulk solution analyses result in at least two-fold better precision for δ^{30}Si (2SD on reference materials ≤0.11 ‰) over that found for the means of *in situ* analyses (2SD typically ≤0.24 ‰).

We find that bushgrass, common reed, and horsetail show large internal variations up to 2 ‰ in δ^{30}Si, reflecting the various pathways of silicon from soil to deposition. fsLA provides a means to identify the underlying processes involved in the formation of phytoliths using silicon isotope ratios.

Keywords

In situ silicon isotope ratios analysis, phytolith, laser ablation inductively coupled plasma mass spectrometry, biogenic silica

Introduction

Silicon is the second most abundant element in the Earth's crust, and considered a beneficial element for plants (Epstein 1999, Marschner and Marschner 2012). Silicon can become highly enriched in plant

tissues (up to 40 $mg \cdot g^{-1}$) where it mainly promotes structural rigidity, pathogen resistance and plant health (Ma and Yamaji 2015, Rodrigues and Datnoff 2015, Deshmukh et al. 2017), and serves to promote to salinity stress resistance (Haghighi et al. 2012, Rios et al. 2017). Silicon is taken up from the soil solution by plant roots exclusively as monosilicic acid (H_4SiO_4) via aquaporin membrane transporters, and is then transported passively along the transpiration gradient towards the plant's organs (Ma et al. 2006, 2011, Delvigne et al. 2009). Silicon is eventually deposited in the form of phytoliths or other amorphous silica precipitates within cell lumina, cell walls or intercellular spaces (Watteau and Villemin 2001, Piperno 2006, Ma et al. 2011). The structure, form, and sizes of phytoliths differ greatly between plant species and can be used to identify their presence from phytoliths preserved in soil and sediment (Piperno 2006). There is an ongoing debate on the stability of phytoliths after their deposition in soil. Fraysse and co-worker showed that the stability of the phytoliths depends on the availability of water, temperature, microbial activity and the acidity of the soil solution, where dissolution is slowest at low pH and low temperature (Fraysse et al. 2006, 2009, 2010). The experimentally determined phytolith dissolution time constant is just slightly lower than that of amorphous silicon. Based on these estimates the half-life of a phytolith with respect to dissolution is between six months and three years (Fraysse et al. 2009). Prentice and Webb showed that during the dissolution of phytoliths, oxygen and silicon isotope are fractionated (Prentice and Webb 2016). The magnitude of the fractionation depends on the pH, and temperature of the solution. The authors observed a two-stage dissolution process. A first, very fast stage that is attributed to the removal of a reactive surface, and a second stage involves re-precipitation of silicon. Under favourable conditions, phytoliths persist dissolution in soil and can be used to reconstruct past vegetation, or the use and domestication of plants during prehistoric settlements (Piperno 2006, Hodson et al. 2008, Hodson 2016).

As is the case for all elements that contain more than one stable isotope, the biogeochemical reactions at the Earth's surface induce a mass-dependent shift in the relative abundance of the three stable silicon isotopes (^{28}Si, ^{29}Si and ^{30}Si). The shift in the resulting isotope ratios can be used to study the biogeochemical cycle of silicon (Bouchez et al. 2013, Sutton et al. 2018). Traditionally, silicon isotope ratios were determined after fluorination of the silicon (either by treatment with a fluorine source (Allenby 1954) or by laser fluorination (De La Rocha et al. 1996) on a gas isotope ratio mass spectrometer (IRMS). Since the 2000s, silicon is analysed in solution using high-resolution MC-ICP-MS. (De La Rocha 2002, Georg et al. 2006). The sample preparation used for the gas IRMS and MC-ICP-MS are designed for bulk analysis and not for the analysis of single phytoliths. The isotopic composition of silicon in plants thus investigated resulted in a large isotopic range of -2.7 ‰ (rice stem) to 6.1 ‰ (rice grains) (Douthitt 1982, Ding et al. 2005, 2008b, 2008a, Ziegler et al. 2005, Opfergelt et al. 2006, 2008, 2010, Engström et al. 2008, Sun et al. 2008, 2016b, 2016a, Hodson et al. 2008, Delvigne et al. 2009,

Köster et al. 2009, Bern et al. 2010, Cornelis et al. 2010, Steinhoefel et al. 2011, Opfergelt and Delmelle 2012, Prentice and Webb 2016, Riotte et al. 2018). Only a few studies investigated the silicon isotope fractionation between plants and soil. Plants preferentially incorporate light silicon, and the isotopic fractionation (reported as $\Delta^{30}Si_{Plant\text{-}Solution}$) for banana, rice and bamboo are between -0.5 ‰ to -1.6 ‰ (Ziegler et al. 2005, Opfergelt et al. 2006, Ding et al. 2008b, 2008a, Sun et al. 2008, 2016b, Delvigne et al. 2009). Apart from the silicon in phytoliths, oxygen has been successfully used as paleoenvironmental proxy. Alexandre and co-worker showed a temperature dependency on the oxygen isotope signature of phytoliths. Changes in the mean annual temperature lead to a shift in the oxygen isotope composition of rainwater, and ultimately those changes are recorded in the silica deposits (Alexandre et al. 2012).

The stable silicon isotope analyses of phytoliths from living plants potentially offers insight into the biogeochemical transformations of silicon between soil and plant organs, whereas the analyses of phytoliths found in soils offer to provide information on their origin and preservation history. An *in situ* analysis technique with a high spatial resolution could in addition provide the possibility to assess phytolith heterogeneity, and thus provide supplemental information on the spatial and temporal variations of the silicon cycles involved. However, to date the application of an *in situ* technique to study stable silicon isotopes of phytoliths is still limited. Steinhoefel and co-worker characterised the different silicon pools in two weathered soils *in situ* to establish an approach to quantify silicon transport processes during weathering. Their investigation included the analysis of the phytolith pool. However, an independent verification of the analytical approach was not performed at that time (Steinhoefel et al. 2011).

To determine *in situ* the silicon isotopic composition of a variety of phytoliths from different plants and thus close this gap, we developed an analytical routine based on femtosecond laser ablation multi collector inductively coupled plasma mass spectrometry (fsLA-MC-ICP-MS). The use of fsLA has been demonstrated to be advantageous for the analysis of stable silicon isotope ratios, in particular when using non-matrix matched reference materials, e.g. (Schuessler and von Blanckenburg 2014). To evaluate our analytical routine, we used a set of natural phytolith samples extracted and purified from soil and a set of phytolith samples extracted directly from plant leaves and stems. Different sample mounting and laser ablation strategies were evaluated to optimise analytical precision. Due to the phytolith's high water and carbon contents matrix effects on instrumental mass bias could potentially arise in the ICP (Jochum et al. 2014, Zheng et al. 2018). Yet no phytolith reference material with a characterised silicon isotope composition is available that would allow the test for such effects. Thus to assess the accuracy of the fsLA-MC-ICP-MS analytical method, comparative values for the natural phytoliths were obtained after bulk digestion, chromatographic silicon purification, and analysis by solution MC-ICP-MS.

Materials and Methods

Phytolith samples

Two different sources for phytoliths were selected. The first source is directly from living plants, and the second source are phytoliths separated from the organic-rich topsoil horizon (O). In total 7 different phytolith samples from 6 different species were collected.

Phytoliths from common reed (Phragmites australis) and bushgrass (Calamagrostis epigejos) were extracted directly from living plants from the "Hühnerwasser" ("Chicken Creek") catchment, the former lignite opencast mine "Welzow-Süd" in northeast Germany (Puppe et al. 2017). Additionally, common and rough horsetail (Equisetum arvense, Equisetum hyemale) were obtained from a location in northern Germany (samples provided by Prof. Peter Behrens, Institute for Inorganic Chemistry, Leibniz University of Hannover). Two different parts of rough horsetail were sampled separately, from annual plants only nodes were calcinated, and from perennial plants the entire stem - containing nodes and internodes were calcinated. Two phytolith samples were extracted from O-horizons of forest soils, i.e. from European beech (Fagus sylvatica L.) collected in Beerenbusch, a study site in northern Brandenburg, Germany, close to the village Rheinsberg (Sommer et al. 2013). Norway spruce (Picea abies) was collected from the Wildmooswald, in the southern Black Forest (Steinhoefel et al. 2011).

With these 7 samples we can investigate the homogeneity of phytolith silicon isotope composition within single plant species. We expect that isotopically homogeneous plant parts will result in a narrow distribution of isotope ratios determined *in situ,* and close agreement between the averages of fsLA with the isotope ratio obtained by solution analysis after bulk sample digestion. Potential heterogeneity within the phytoliths is expected to result in a broader silicon isotope ratio distribution obtained from fsLA. Depending on how representative the phytolith fragments selected for *in situ* analyses are, a deviation in the isotope averages of fsLA ratio from the isotope ratio from bulk solution will emerge. Such a deviation can also be caused by samples that contain sub-micrometre sized silicate precipitates (Sommer et al. 2006). These would be contained in bulk analyses, but not in the larger fragments mounted for fsLA. For phytoliths extracted from soil (Norway spruce and European beech) such differences are not expected, as during the sample preparation an amalgamation of fragments is taking place which leads to an artificial homogenisation of Si pools and their of isotope ratios.

Phytolith extraction

Phytoliths sampled directly from the plant parts were ashed at 600°C (6 – 24h). European beech and Norway spruce phytoliths were extracted from the organic-rich forest soil layer by combined chemical and physical separation procedure. Those phytoliths were extracted by oxidising the organic matter using H_2O_2 (35 vol%), HNO_3 (65 vol%), $HClO_4$ (70 vol%) at 80 °C until reaction subsides. Subsequently,

Fe oxides and carbonates are dissolved by boiling the sample in HCl (10 vol%) for 30 min. Finally, the phytoliths are separated by shaking the remaining solid phase with 30 mL of sodium polytungstate ($Na_6(H_2W_{12}O_{40})\cdot H_2O$, density of 2.3 $g\cdot cm^{-3}$), centrifugation at 3000 rpm for 10 min, carefully pipetting the supernatant, and filtering by 5µm Teflon filter. This step was repeated three times. The filter residue was washed with water, and dried at 105 °C. (Alexandre et al. 1997, Sommer et al. 2013). The obtained phytolith separates are compacted into a loosely bound pellet (see Phytolith imaging section) and might contain minor amounts of residual quartz, clay, or particles from aeolian dust (Steinhoefel et al. 2011).

Phytolith imaging

For sample characterisation, phytoliths were imaged using a scanning electron microscope (SEM, Zeiss Ultra Plus, working distance 7.6 mm, acceleration voltage 15 kV) and a light microscope (Leica EZ4D) at GFZ Potsdam. The phytoliths imaged by SEM were fixed on an aluminium holder using carbon-conductive adhesive tape and were carbon-coated. For light microscopy the phytoliths were mounted with the same method as used for LA, fixed with lacquer on a microscope slide.

Sample preparation for laser ablation

Three different strategies for introducing mounted phytoliths into the ablation cell were evaluated. In the first strategy phytolith fragments were imbedded in epoxy resin. The mount was carefully polished to expose the fragments. In the second method phytoliths were directly fixed by carbon-conductive adhesive tape onto an aluminium SEM holder. In the third method phytolith samples were fixed onto microscope slides using clear nail lacquer.

The preparation of the epoxy mounts is time consuming, and part of the sample is lost in the polishing process. The resulting thin sample will eventually lead to shorter measurement duration, and thus to lower precision in isotope ratios. Sample preparation on adhesive tape is faster. Phytoliths immediately adhere to the aluminium holder and can be analysed directly by LA. However, adhesive tape tends to attract dust and laser debris. Nail lacquer performs similarly to adhesive tape, dries in 40 s, and the entire phytolith can be analysed. To minimise possible contamination from the support, microscope slides made from poly(methyl methacrylate) (PMMA) were used throughout the study. Several commercial nail polishes and lacquers were bought in a local German chemist's shop and tested for blank contamination, impact and scrub resistance. An advantage of nail lacquer is that phytoliths can be recovered by re-dissolving the lacquer.

Method validation strategy and uncertainty evaluation

No phytolith reference material with a characterised silicon isotope composition is available for use as external reference material. Since phytoliths are made up of bio-opal, they contain water (<9%) and to

some extent also carbon (Piperno 2006). The presence of carbon potentially leads to matrix effects in the plasma, which would not be accounted for using the standard sample bracketing approach with a dry reference material containing no carbon (Fliegel et al. 2011, Frick and Günther 2012). Moreover, the material embedding the phytoliths (epoxy resin or nail laquer) might get partially ablated. To evaluate the performance of the silicon isotope measurements obtained by fsLA-MC-ICP-MS, several reference materials (BHVO-2, NBS28) and a homogenised phytolith sample (European beech) were analysed by both fsLA-MC-ICP-MS and bulk solution MC-ICP-MS, respectively. Additionally, reference materials for which published silicon isotope data exists (ATHO-G, BHVO-2, GOR132-G, and NIST612) were analysed in each fsLA session for quality control and to verify that the target measurement uncertainty is met. Thereby uncertainties in the measurement results of these homogenous materials can be evaluated and then used as a benchmark to assess micro-scale silicon isotope heterogeneity in the unknown phytolith samples detected by *in situ* fsLA-MC-ICP-MS analysis.

The silicon isotope results are reported in the δ-notation as permil deviation relative to an international measurement standard (Coplen et al. 2002).

$$\delta^{30}Si = \left[\frac{\left(\frac{^{30}Si}{^{28}Si}\right)_{sample}}{\left(\frac{^{30}Si}{^{28}Si}\right)_{standard}} - 1 \right] [in\ ‰] \quad (1)$$

All δ^{29}Si and δ^{30}Si from bulk solution MC-ICP-MS analysis are reported relative to NBS28 (quartz NIST SRM8546 alias NBS28, $\delta^{29}Si \equiv 0$ and $\delta^{30}Si \equiv 0$; directly used as bracketing measurement standard) and *in situ* fsLA-MC-ICP-MS analysis are reported relative to NIST SRM610 (used as bracketing measurement standard) which is isotopically indistinguishable from NBS28, and also identical to NIST SRM612 (Schuessler and von Blanckenburg 2014, and Table S7)

All δ^{30}Si and δ^{29}Si results are accompanied with uncertainties at the 95% confidence level, exemplified for δ^{30}Si as follows. Individual δ^{30}Si values obtained by *in situ* analysis by fsLA-MC-ICP-MS contain mainly three uncertainty contributions, i.e. from the analysis of the sample and from the two bracketing standard measurements (NIST SRM610). For each of these, an expanded standard measurement uncertainty (U) (JCGM 2008) is obtained by calculating the standard deviation (s) of n silicon isotope ratio integration cycles acquired during < 3 min of analysis ($18 > n < 94$ for samples given in Frick et al. 2018, Table S1). Count- statistical uncertainties at the 95% confidence level can be expressed as the standard deviation of the mean ($2 \cdot s_m = \frac{k \cdot s}{\sqrt{n}}$) with a coverage factor k = 2 (Ellison and Williams 2012). Here, instead of k we use t derived from student-t distribution at 95% confidence to account for variable n ($2SE = \frac{t \cdot s}{\sqrt{n}}$; this is also sometimes called the standard error of the mean at 95% confidence). By propagation of these individual counting statistical uncertainties through equation 1,

198 we obtain a combined expanded standard uncertainty (U_c) for each individual *in situ* fsLA-MC-ICP-MS
199 δ^{30}Si result. We note that other components of variance contributing to the uncertainty (e.g., mass
200 bias stability, blank correction, …) are already included in this statistical evaluation.

201 To evaluate the measurement precision the repeatability was calculated as 2 times the standard
202 deviation (2SD) of n individual δ-values obtained by independent sample-standard bracketing
203 measurements. We followed this procedure on reference materials of which the average results and
204 their uncertainties were compared to independently obtained δ^{30}Si values, and to verify the previously
205 established target uncertainty of the fsLA-MC-ICP-MS method of better than ±0.23‰ (2SD) and
206 ±0.15‰ (2SD) for δ^{30}Si and δ^{29}Si, respectively (Schuessler and von Blanckenburg 2014, Frick et al.
207 2016).

208 The latter approach is also used for bulk solution MC-ICP-MS silicon isotope analysis, where repeat
209 measurements of samples and reference materials (after dissolution and silicon chromatographic
210 purification) are obtained and average δ^{30}Si and δ^{29}Si values and associated standard deviations are
211 calculated (Table 1 and S6).

212 To obtain reference silicon isotope ratios for our laser ablation study we have measured bulk phytolith
213 samples after dissolution using an established alkali fusion method (Georg et al. 2006, Zambardi and
214 Poitrasson 2011, Schuessler and von Blanckenburg 2014). Briefly, 5 to 15 mg phytoliths were fusion
215 melted in an Ag crucible with NaOH (p.a. grade, tested for silicon background levels) at 750°C for
216 15 min. The fusion cake was dissolved in ultra-pure water (18 MΩ·cm) followed by mild 0.03 M HCl.
217 The obtained solution was acidified to pH 1.5 with HCl. An aliquot of the solution was loaded onto
218 chromatography columns (Spectrum 104704 PP containing 1.5 ml AG50W-X8) and silicon was eluted
219 with 5 ml H_2O. Complete silicon recovery and purity (> 95% Si) was verified by ICP-OES analysis. Before
220 MC-ICP-MS analysis, the purified silicon solutions were acidified to 0.1 M HCl and diluted to a
221 concentration of 0.6 $\mu g \cdot g^{-1}$. Solutions of samples and bracketing measurement standards (NIST
222 SRM8546, NBS28) were both doped with 0.6 $\mu g \cdot g^{-1}$ Mg to use the $^{25}Mg/^{24}Mg$ ratio for mass bias drift
223 correction during the analysis. The solutions were introduced into the ICP using an ESI ApexHF
224 desolvator and a self-aspirating PFA nebuliser (measured uptake 160 $\mu L\ min^{-1}$). Measurements were
225 done in dynamic mode, alternating between silicon and magnesium isotopes, each for 30 cycles at 4 s
226 integration time per cycle. The Neptune cup configuration and instrument settings can be found in the
227 supplement, Table S1 and Table S2. BHVO-2 (USGS, basalt powder) is a well-characterised reference
228 material for silicon isotopes and was prepared and analysed together with the phytoliths to verify no
229 bias is introduced during sample preparation and measurement. Additionally, ERM-CD281 (IRMM, rye
230 grass) was analysed using the same method; unfortunately up-to-now, there are no other published
231 silicon isotope data available for comparison. All δ^{29}Si and δ^{30}Si from bulk analysis are reported relative

to NBS28. Since NIST SRM610 and NBS28 are isotopically indistinguishable in their silicon composition, the bulk and *in situ* data can be directly compared (Schuessler and von Blanckenburg 2014, Frick et al. 2016, Table S7).

In situ silicon isotope analysis by femtosecond laser ablation MC-ICP-MS

In situ silicon isotope ratios were measured using a custom-built deep-UV (196 nm) femtosecond laser ablation system (*GFZ fem2*, containing a frequency-quadrupled Spectra Physics Solstice femtosecond laser, see (Schuessler and von Blanckenburg 2014) for technical details) in combination with an inductively coupled plasma multi-collector mass spectrometer (Thermo Fisher Scientific Neptune MC-ICP-MS, equipped with the Neptune Plus Jet Interface) at the Helmholtz Laboratory for the Geochemistry of the Earth Surface (von Blanckenburg et al. 2016). The ion optics were operated at medium mass resolution with a typical mass resolving power $m/\Delta m > 6000$, to resolve isobaric interferences (mainly $^{14}N^{16}O^{+}$ on $^{30}Si^{+}$). Faraday detectors (equipped with 10^{11} Ω amplifiers) were positioned to measure on interference-free, flat top peak shoulders. The Faraday cup configuration is shown in Table S3. The gas flows, torch position, and ion optics were tuned daily for highest intensity and mass bias stability, while maintaining the $^{14}N^{16}O^{+}$ interference on $^{30}Si^{+}$ at resolvable levels (<10 V). The typical laser and ICP-MS settings can be found in Table S4 and Table S5.

fsLA has proven to be advantageous over nsLA for non-matrix matched silicon isotope ratio standardisation of different sample matrices (Janney et al. 2011, Schuessler and von Blanckenburg 2014). To further improve the mass bias stability during non-matrix matched calibration using the standard-sample-bracketing approach, wet plasma conditions were used by admixture of water from spray chamber nebulisation to the laser aerosol before entering the ICP. The addition of water stabilises the position of the highest analyte ionisation density in the plasma regardless of the matrix, which leads to an improved accuracy in non-matrix matched quantification (Flamigni et al. 2012, 2014). Both measures, fsLA and wet plasma lead to less mass bias drift between bracketing standards and samples and thus improves the precision of the isotope ratio determination. Instrumental mass bias was corrected for by standard-sample-bracketing using NIST SRM610 as measurement standard (Frick et al. 2016). The laser beam (ca. 25 µm in diameter) on the sample was continuously scanned over the sample - the paths were adapted to the irregular shapes of phytolith samples. To account for the fragile nature and sometimes also porous structure of phytoliths, the laser frequency (pulse repetition rate) during phytolith analysis was dynamically adjusted to maintain a signal intensity as similar as possible to that obtained during ablation of the bracketing standard (4 - 7 V on ^{28}Si). Moreover, every analytical session contained a range of reference materials (ATHO-G, BHVO-2, GOR132-G, NIST SRM612, and NBS28) that were repeatedly analysed in between the phytolith measurements for comparison to published values (see compilations in (Jochum et al. 2005, Schuessler and von Blanckenburg 2014).

Raw data processing and background corrections were made according to the protocol described in Schuessler and von Blanckenburg (2014) that also involves application of several data rejection/acceptance criteria. Of these, the most important ones are that A) only $^{30/28}$Si and $^{29/28}$Si ratios are used for the calculation which deviate less than 3SD from the mean and B) only results which follow the mass-depended terrestrial fractionation line in a three-isotope-plot of δ^{29}Si vs. δ^{30}Si within analytical uncertainties and C) have a mass bias drift between the two bracketing standards of less than 0.30 ‰ in $^{30/28}$Si are accepted and reported in this study.

Results and Discussions

Phytolith imaging

In Figure 1 SEM and optical microscopic images of the phytolith samples are shown with typical laser ablation paths. Phytoliths from rough horsetail look like sheet structures. Figure 1A and 1B show SEM images of the epoxy embedded (A) and carbon tape-affixed (B) perennial horsetail sample. In Figure 1A the thin nature of the sheet structures is visible. In Figure 1B a group of intact stomatal phytoliths after the separation process are shown. For comparison, Figure 1C shows the optical microscopic image of the perennial horsetail phytoliths sample affixed using nail lacquer.

The annual and perennial rough horsetail phytolith samples differ by the age of the plants and by the plant parts from which they were extracted. The perennial sample consist of stems and nodes, and the annual sample are from nodes only. No visual difference between the nodes of the annual and perennial sample was visible. Common horsetail phytoliths (not shown) form also sheet-like structures.

European beech and Norway spruce phytolith samples were separated from forest soils. Figure 1D shows the optical microscopic image of the Norway spruce phytolith sample and Figure 1E-F of European beech. Figure 1E reveals a compacted particle structure that resulted from the chemical and physical sample separation employed. The sample comprises a mixture of phytolith fragments rather than a single phytolith.

Common reed phytoliths form are also sheet-like structures (Figure 1G), however the sheets tend to be smaller and thinner compared to the rough and common horsetail samples. Typically, only one to two laser ablation passes were possible before exhausting the sample. To ensure sufficient analysis time nevertheless the size of the ablation area was increased. The bushgrass phytolith sample (Figure 1H) is an assembly of small sheet like structures (300-400 µm) with much smaller fragments (10 µm) of various sizes and shapes.

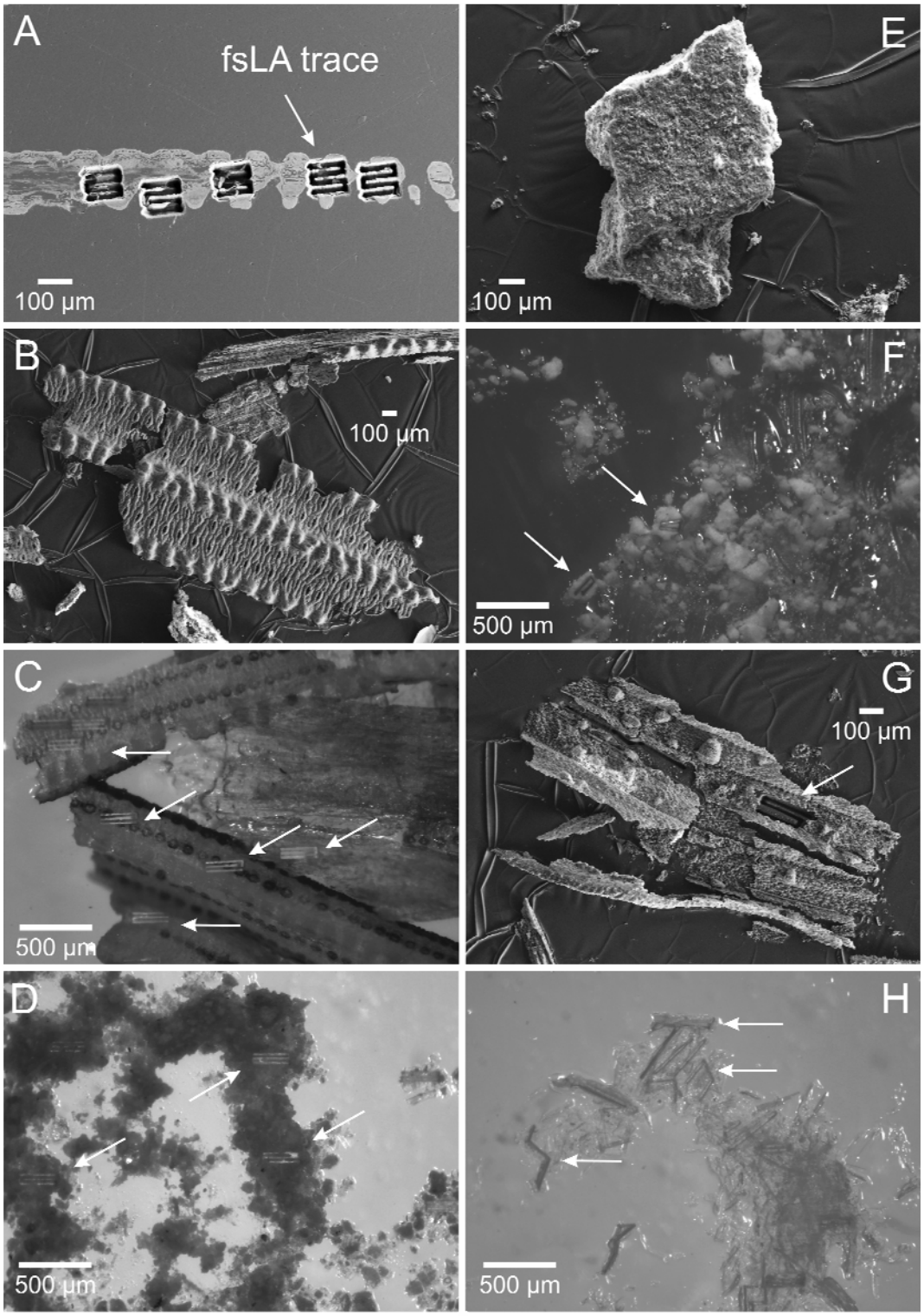

Figure 1: SEM (A,B,E, and G) and optical microscopy (C,D,F, and H) images of the phytolith samples. (A-C) rough horsetail, (D) Norway spruce, (E-F) European beech, (G) common read, and (H) bushgrass phytoliths. (A-C) shows the different fixation techniques used in this study, (A) embedded into epoxy, (B) affixed using carbon sticky tape, (C) affixed using nail lacquer. (D-F) shows the compact, pellet-like nature of the Norway spruce and European beech phytoliths separated from the forest soil. Common reed (G), and (H) bushgrass phytoliths show a sheet-like structure. Scale bars are 100 µm for SEM, and 500 µm for the light microscopy images. Apart from (B) and (E) the images show typical laser ablation traces which are highlighted with white arrows.

Bulk phytolith silicon isotope analysis results

The bulk silicon isotope ratio composition of the 7 samples measured by solution MC-ICP-MS (after fusion digestion and chromatographic silicon purification) ranges from $\delta^{30}Si$ = -1.12 ‰ to +1.27 ‰ (see Table 1). This is within the range previously reported in the literature for phytoliths ($\delta^{30}Si$ -2.3 to +6.1 ‰) (Douthitt 1982, Ding et al. 2005, 2008b, 2008a, Ziegler et al. 2005, Opfergelt et al. 2006, 2008, 2010, Engström et al. 2008, Sun et al. 2008, 2016b, 2016a, Hodson et al. 2008, Köster et al. 2009, Bern et al. 2010, Cornelis et al. 2010, Steinhoefel et al. 2011, Opfergelt and Delmelle 2012, Prentice and Webb 2016). The values reported in the literature however, comprise not only of samples from natural ecosystems, but also from laboratory growth experiments, and included samples from roots to seeds, and some examples were analysed by fluorination and gas MS which might have resulted in lower accuracy than modern solution MC-ICP-MS techniques.

*Table 1: Silicon isotope ratios from bulk phytolith digestion, with 2 standard deviations based on n replicate mass spectrometer measurements. For in situ fsLA, standard deviation is based on n measurement of individual phytoliths. *Bushgrass was digested and analysed in two independent bulk solution MC-ICP-MS analytical sessions (each n=3). †Norway spruce sample was analysed previously by* (Steinhoefel et al. 2011) *and resulted in $\delta^{30}Si$ = -0.36 ± 0.09 ‰. The measurement standards NBS-28 and NIST SRM610 are indistinguishable in their silicon isotope composition and therefore delta values from both analytical techniques can be directly compared.*

	Bulk digestion solution MC-ICP-MS					***In situ* fsLA-MC-ICP-MS**					
Sample	**$\delta^{29}Si_{NBS28}$ (‰)**	**2SD**	**$\delta^{30}Si_{NBS28}$ (‰)**	**2SD**	**n**	**$\delta^{29}Si_{NIST610}$ (‰)**	**2SD**	**$\delta^{30}Si_{NIST610}$ (‰)**	**2SD**	**n**	**Range of individual $\delta^{30}Si_{NIST610}$ (‰)**
Bushgrass*	0.50	0.07	0.99	0.12	6	0.12	1.15	0.24	2.17	33	-1.23 – 3.85
Common horsetail	-0.56	0.15	-1.12	0.23	3	-0.40	0.95	-0.74	1.78	11	-2.92 – 0.48
Common reed	0.66	0.07	1.27	0.05	3	0.50	1.16	1.06	2.16	18	-0.05 – 4.26
European beech	0.08	0.10	0.13	0.09	3	0.04	0.17	0.10	0.24	24	-0.12 – 0.39
Norway spruce†	-0.21	0.03	-0.42	0.07	3	-0.08	0.75	-0.15	1.42	24	-0.88 – 1.39
Rough horsetail (annual)	0.06	0.03	0.14	0.06	3	-0.24	0.63	-0.44	1.20	18	-2.34 – 0.19
Rough horsetail (perennial)	0.32	0.07	0.61	0.13	3	0.24	0.73	0.43	1.40	21	-0.85 – 1.45

Two different reference materials, BHVO-2 and ERM-CD281, were analysed using the same procedure along with the phytolith samples. The results are shown in the supplement, Table S6. Within two standard deviations there is no difference between the measured and the published values (Jochum et al. 2005, Schuessler and von Blanckenburg 2014). The repeatability of all solution MC-ICP-MS measurements on samples and reference materials is similar to what was previously obtained using this method (Tatzel et al. 2015, Oelze et al. 2016, Frick et al. 2016).

Results of *in situ* phytolith analysis

Evaluation of the laser ablation parameters and sample preparation methods

The fsLA system employed in this study is characterised by two features that differ from those common to ns lasers. The achievable spot size is limited to 15-30 µm, and the laser beam has a Gaussian energy

distribution. Both the small spot size and the Gaussian intensity distribution result in rapid increase in laser crater depth which is accompanied by fast decrease in ion beam intensity. We circumvent this effect by three means. A) We typically perform a small-size raster (50 · 100 µm) analysis instead of a single spot analysis; B) in contrast to nsLA we use a faster scan speed (40 µm/s); and C) we employ a higher laser pulse repetition rate (frequency 20-40 Hz). During the optimisation of the analytical routine we evaluated laser parameters optimised for the different phytolith types. For the sheet-like structured phytoliths from common and rough horsetail, a larger raster or line scan across selected features was chosen. During the first pass on those sample, a low laser pulse repetition rate (15-20 Hz) was applied to obtain signal intensities in the range of 4-7 V for ^{28}Si. On the subsequent passes the laser frequency was increased. The ablation characteristics of the compacted phytolith samples, European beech and Norway spruce, resembled closely those encountered on silicate glass reference materials. These samples were analysed with a small raster size, with up to 10 passes and without the need to adjust the laser frequency. Generally, we have chosen analysis parameters similar to those outlined by Schuessler and von Blanckenburg, with laser ablation durations of 100 s, and on-peak background measurements after each sample (Schuessler and von Blanckenburg 2014).

Three different strategies for fixing the phytolith samples in the ablation cell were evaluated. Embedding samples into epoxy resin typically led to short data acquisition periods at ion beam intensities that provide good counting statistics with high temporal variations in signal intensity (Figure 2). This is mainly due to the relatively thin samples left after polishing the epoxy mounts that are consumed while the laser ablation pit deepens with every pass of the line scan and also ablates areas consisting predominately of epoxy resin where the porous sample has been removed by polishing. In contrast, affixing phytoliths using adhesive tape or clear nail lacquer does not lead to a loss of material. This leads to longer data acquisition periods at a relatively constant signal intensity, resulting in a better precision of the silicon isotope ratios. An example for this different ablation behaviour is shown in Figure 2. Figure 2A-B is a rough horsetail (perennial) phytolith imbedded into epoxy, and Figure 2C-D fixed with nail lacquer on a PMMA slide.

The signal on the epoxy-embedded phytoliths appears only after the third pass of the laser ablation raster (see Figure 2A). During the first two passes the phytolith was still partially covered with epoxy. The laser pulse repetition rate (frequency) was thus increased to accelerate the ablation. Once the phytolith was fully uncovered, very high signal intensities were recorded. For the nail lacquer-fixed phytolith, such initial uncovering was not required, and the ion signal was detected shortly upon ablation began and remained stable throughout the analysis. The signal on the epoxy-embedded phytolith lasted for about 50 seconds, whereas for the phytolith fixed with nail lacquer the full ablation period of 100 s was used for data acquisition. The epoxy-embedded perennial rough horsetail analysis resulted in a $\delta^{30}Si = 0.87 \pm 0.25$ ‰ (n = 56, 2 SE) and for the nail lacquer-fixed phytolith 0.86 ± 0.18 ‰

(n = 81, 2 SE). The average $\delta^{30}Si$ by bulk solution MC-ICP-MS result is 0.61 ± 0.13 ‰ (n = 3, 2SD) and the average fsLA-MC-ICP-MS result for this sample is 0.43 ± 1.40‰ (n = 21, 2SD).

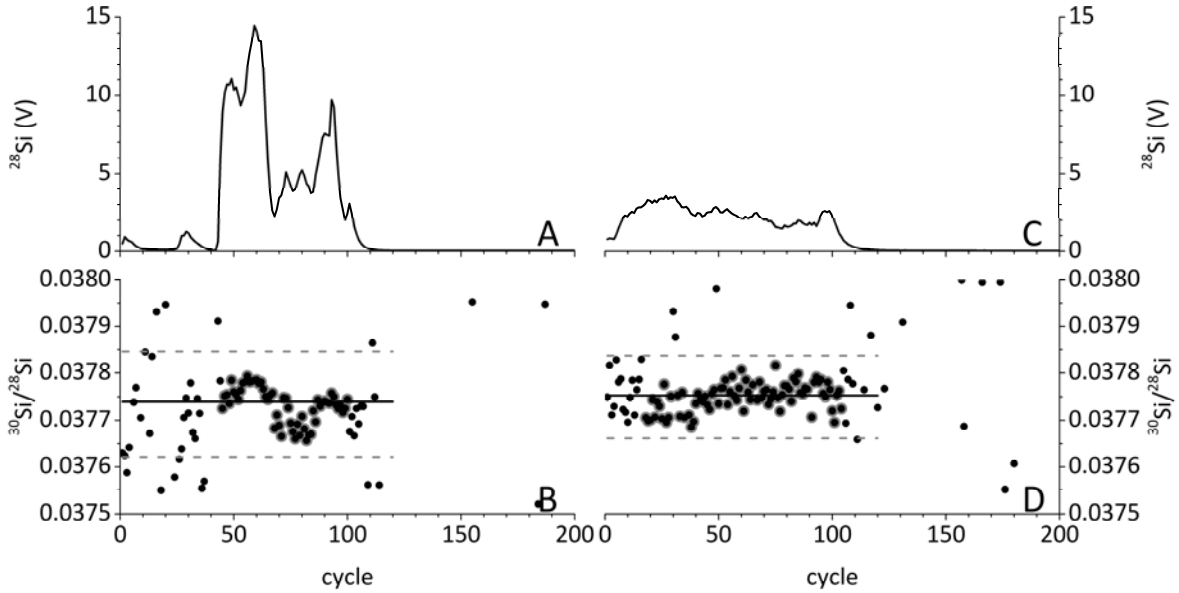

Figure 2: Typical fsLA-MC-ICP-MS signal from rough horsetail (perennial) phytoliths, left (A-B) embedded in epoxy resin, and right (C-D) glued with clear nail lacquer. ^{28}Si intensity (A, C), $^{30/28}Si$ ratio (B, D), and calculated mean (solid black line) with 3 SD (dashed grey line) of the $^{30/28}Si$ ratio (black dots). Only $^{30/28}Si$ ratios that are deviating less than 3 SD from the mean in their $^{30/28}Si$ and $^{29/28}Si$ ratio are used for the data evaluation and calculation of delta values (grey circles). For clarity, background ratios (acquired beyond 120 cycles) are not shown. One cycle is equal to an integration time of 1.049 seconds.

Carbon-adhesive tape and nail lacquer are our preferred sample preparation methods. The preparation is faster, and a smaller number of preparation steps are involved. However, when handling the sample, the epoxy-embedded and nail lacquer-fixed samples are favoured, since no dust or laser ablation debris can adhere to the sample after the epoxy or lacquer has dried. Based on these considerations the best applicable sample preparation method is using clear nail lacquer to affix the phytolith samples onto PMMA slides.

Evaluation and comparison of fsLA with the bulk solution silicon isotope measurements

The results of the *in situ* measured phytoliths by fsLA-MC-ICP-MS are shown in Figure 3, and the individual results are reported in Table S1 in the accompanying data publication (Frick et al. 2018). Each phytolith sample was analysed in at least three independent measurement sessions. Data in Figure 3 are sorted according to the measurement session.

Comparing $\delta^{30}Si$ values from bulk solution MC-ICP-MS silicon isotope with the averages from *in situ* fsLA-MC-ICP-MS analysis, three different cases can be identified. A) A heterogeneous silicon isotope composition of phytoliths within a single plant species (bushgrass, common reed, rough horsetail, and common horsetail), B) a homogeneous composition from the soil-extracted phytoliths (European beech) and C) a heterogeneous composition from the soil-extracted phytoliths of Norway spruce. The potentially existing fourth case, a homogenous distribution of phytoliths from a single plant species,

was not found. The wide variation in silicon isotope ratios of more than 2 ‰ observed within a single plant indicates that different silicon translocation and utilisation mechanisms in the plant are traced by silicon isotopes. The soil water silicon isotopic composition as well as the cell environment, where silicic acid is dehydrated and phytoliths are formed, influence the isotopic composition of the formed phytoliths. For common reed, rough horsetail (perennial) and common horsetail no systematic bias between the bulk solution and *in situ* fsLA data is observed. For bushgrass and rough horsetail (annual) a systematic difference between results from both measurement methods is apparent. Closer inspection of the distribution of the single bushgrass phytolith analysis indicates, however, that this difference is not due to a systematic analytical bias. Rather, while the large spread is due to inter-phytolith fragment isotopic heterogeneity, the small number of phytoliths analysed by fsLA-MC-ICP-MS did not result in representative sampling of the distribution. For the annual rough horsetail phytolith sample, the individual micro-scale analysis overlaps with the bulk analysis within uncertainties. A systematic offset between the two analytical routines is therefore unlikely. These results together with the results obtained on reference materials (Table S7, supplement) verify the previously established target uncertainty of the fsLA-MC-ICP-MS method of better than ±0.23‰ (2SD) and ±0.15‰ (2SD) for $\delta^{30}Si$ and $\delta^{29}Si$, respectively (Schuessler and von Blanckenburg 2014, Frick et al. 2016).

For European beech and Norway spruce an amalgamation of the phytoliths has taken place during the extraction procedure from the soil horizon and separation. The phytolith samples of European beech show a very narrow silicon isotope ratio distribution, indicating either a homogenisation of the silicon isotopic composition during the sample preparation, or a homogeneous initial phytolith composition. The electron microscope image showed finely-ground material (see Figure S1A in the supplement). Thus, homogenisation during sample preparation is the most likely explanation. The average silicon isotope composition obtained by fsLA-MC-ICP-MS ($\delta^{30}Si = 0.10 \pm 0.05$ ‰, combined expanded standard uncertainty at 95% CI for n = 24) overlaps within the confidence interval of the average bulk solution MC-ICP-MS result ($\delta^{30}Si = 0.13 \pm 0.11$ ‰, n = 3) for this sample. For Norway spruce the measured micro-scale silicon isotopic variability is higher ($\delta^{30}Si$ = -0.88 to +1.39 ‰), and here, phytoliths fragments observed by SEM are larger (see Figure S1B in the supplement), indicating that a small-scale homogenisation of the fragments has not been attained. Close inspection of the individual fsLA-MC-ICP-MS results for Norway spruce reveals that a small number of phytoliths in the sample population are significantly heavier in their silicon isotope composition than the bulk composition (up to $\delta^{30}Si = 1.39$ ‰). The detection of such small sub-groups within a sample population is one of the strengths of the *in situ* technique and would not have been noticed in the bulk solution MC-ICP-MS analysis. The average Norway spruce fsLA-MC-ICP-MS result ($\delta^{30}Si = -0.15 \pm 0.30$ ‰, n = 25) and the bulk silicon isotope composition ($\delta^{30}Si = -0.42 \pm 0.09$ ‰, n = 3) are indistinguishable from each other

within their uncertainties. We conclude that for the two most homogeneous samples (Norway spruce and European beech) no systematic difference between the two analytical methods is apparent. Thus, the fsLA-MC-ICP-MS analytical routine can provide accurate *in situ* stable silicon isotope ratios of plant and soil extracted phytoliths. Any systematic differences between *in situ* and bulk silicon isotope ratio signatures thus arises from non-representative sampling, such as the possible inclusion of sub-micrometre sized silicate precipitates in bulk samples and their exclusion from larger phytolith samples which were not amalgamated.

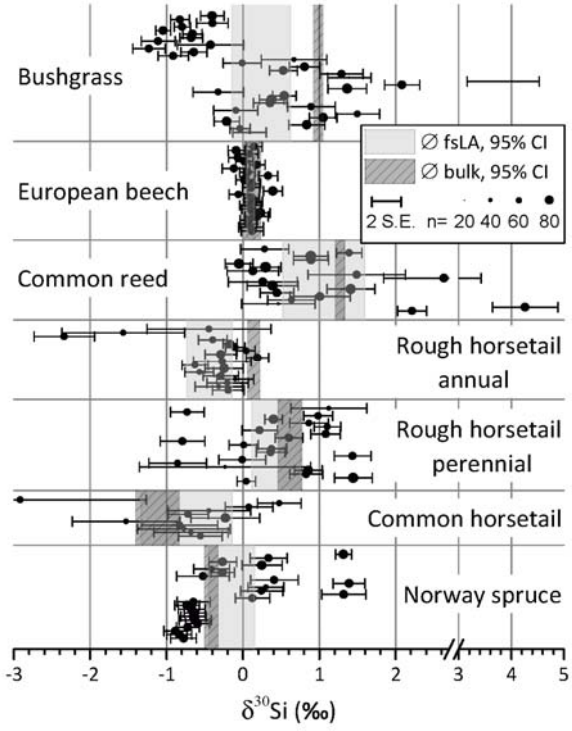

Figure 3: $\delta^{30}Si$ values measured by in situ fsLA-MC-ICP-MS on phytolith samples (bushgrass, European beech, common reed, rough horsetail, annual and perennial, common horsetail and Norway spruce). Uncertainty on each individual data point is the combined expanded standard uncertainty at the 2SE level for $\delta^{30}Si$ (see method section for definition). Light grey area is the average $\delta^{30}Si$ value (relative to NIST SRM610) for each sample from in situ fsLA-MC-ICP-MS analysis with 95 % confidence interval. The dark grey shaded area is the average $\delta^{30}Si$ composition (relative to NBS28) with 95 % confidence interval obtained by bulk solution MC-ICP-MS. The size of the data points is indicative of the number of measurements cycles used for data acquisition (1 cycle = 1.049 s integration time). Only where few cycles were acquired (<30 integrations) the statistical uncertainty expressed as $\frac{t \cdot s}{\sqrt{n}}$ increases. The measurements are arranged according to the temporal sequence in which they were measured. The results include phytoliths from epoxy-embedded, nail lacquer-, and carbon-adhesive fixed specimens.

Analytically the *in situ* analysis of the phytolith samples is more challenging due to non-uniform ablation behaviour resulting in higher uncertainties compared to the analysis of glass or rock reference standards. The non-uniform ablation causes individual integration cycles to strongly deviate from the mean. These can be identified by a statistical outlier test and rejected. For analysis where more than forty 1-second-integration cycles were averaged, no systematic variation with the standard deviation of the mean is observed. For very short data acquisition periods (n < 30, see dot size in Figure 3) we observe an increase in the standard deviation of the mean in silicon isotope ratios for an individual analysis, and thus an increase in the combined expanded standard uncertainty of $\delta^{30}Si$ values. Some

of the results are subject to a large analytical uncertainty, which span almost the entire reported silicon isotopic range of biogenic opal. For completeness those data are included in Figure 3, in the following discussion those inferior data are however omitted.

Implications for silicon biogeochemistry

The *in situ* fsLA-MC-ICP-MS results allow to develop a more detailed insight into the biogeochemistry of silicon in plants. The first significant finding is the small-scale heterogeneity in the silicon isotope composition within a given plant species (Figure 4). Not only does this heterogeneity imply that a variety of processes are involved in the formation of phytoliths in plants. The obtained isotope ratios potentially also aide to identify these processes.

Results from both annual and perennial rough horsetail samples are good examples of this potential application. The bulk analyses reveal a significant difference between the annual and the perennial sample. The annual phytoliths show a lower δ30Si signature (0.14 ± 0.06 ‰, 2SD) than the perennial phytoliths (0.61 ± 0.13 ‰, 2SD). For these differences three explanations are possible: A) differences in soil chemistry can result in a compositional change in the plants' silicon source; B) the isotope fractionation during uptake varies, depending on environmental conditions; and C) the removal of stems in the annual sample shifts the isotopic composition. All three explanations will result in differences in the silicon isotope composition of the formed phytoliths. Note that explanations A) and B) might also include temporal variations, as the isotope composition of silicon in the source may shift between years but also between seasons (Steinhoefel et al. 2017), and so may the isotope fractionation factors depending on, for example, silicon saturation in fluids or pH. Thus δ^{30}Si of individual fragments might depend on their age. Given the experimental design, a differentiation between the three mechanisms are not possible.

We also find specific silicon isotope ratios that appear to correlate to morphological features of analysed phytoliths. Optical microscopy imaging of laser ablation paths in the perennial horsetail sample revealed that the two analyses with the horsetails' lowest δ^{30}Si (-0.79 ‰ and -0.85 ‰) were measured in a region lacking visible features of stomata. In all other measurements, yielding higher δ^{30}Si, the laser ablation path included stomata features. This distinction suggests differences in the depositional processes of bio-silica close to stomata, or that these particular phytoliths were formed at a different stage of the plants growth and thus from a different source of silica.

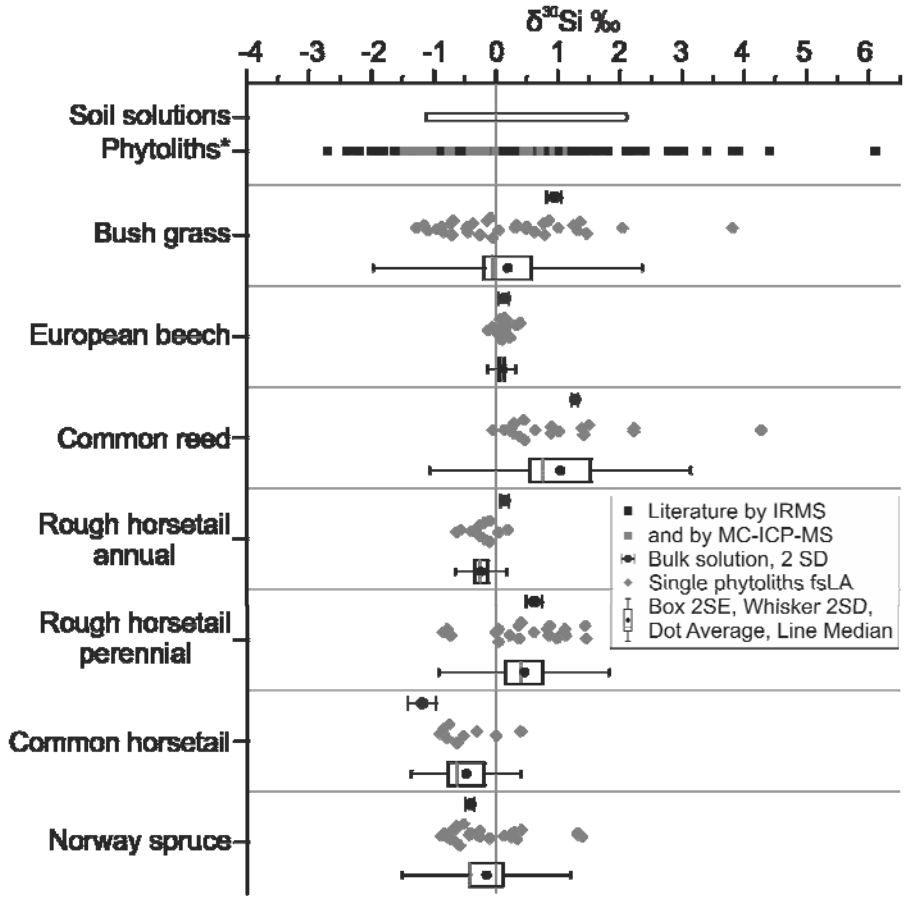

481

482 *Figure 4: δ^{30}Si values of the analysed phytoliths. Black circles denote bulk solution MC-ICP-MS results, error bars are 2SD of*
483 *repeated measurements. Grey diamonds denote single values determined by fsLA-MC-ICP-MS. Box plots depict mean (black*
484 *dot) and median (dotted line) of the in situ fsLA-MC-ICP-MS measurements, with 2 standard error (box size) and 2 standard*
485 *deviation (whisker). For comparison the top row contains the Si isotope range of published soil solutions* (from Opfergelt and
486 Delmelle 2012) *and published values for phytoliths and biogenic opal are shown in black (measured by gas phase IRMS) and*
487 *grey (measured by MC-ICP-MS).* (Douthitt 1982, Ding et al. 2005, 2008b, 2008a, Ziegler et al. 2005, Opfergelt et al. 2006, 2008,
488 2010, Engström et al. 2008, Sun et al. 2008, 2016b, 2016a, Hodson et al. 2008, Delvigne et al. 2009, Köster et al. 2009, Bern
489 et al. 2010, Cornelis et al. 2010, Steinhoefel et al. 2011, Opfergelt and Delmelle 2012, Prentice and Webb 2016, Riotte et al.
490 2018)

491 The second finding that highlights the future scientific potential of this method is a higher δ^{30}Si in some
492 of the phytoliths (Figure 4) compared to the δ^{30}Si of typical soil solutions that range from -1 to +2 ‰
493 (Opfergelt and Delmelle 2012). Plants preferentially incorporate light silicon isotopes from the soil
494 solution, with a ^{30}Si/^{28}Si fractionation between plant and soil solution of -0.5 ‰ to -1.6 ‰ (Ziegler et
495 al. 2005, Opfergelt et al. 2006, Ding et al. 2008b, 2008a, Sun et al. 2008, 2016b, Delvigne et al. 2009)
496 such that δ^{30}Si of around 0 ‰ is expected for whole plants. Bushgrass and common reed were
497 harvested from the same catchment, and both yielded a significantly heavier silicon isotope signature
498 ($\delta^{30}Si_{bulk}^{bushgrass}$ = 0.99 ± 0.12 ‰, and $\delta^{30}Si_{bulk}^{common\ reed}$ = 1.27 ± 0.05 ‰, with an outlier of 3.85 ± 0.69 ‰
499 in bushgrass, and another outlier of 4.26 ± 0.58 ‰ in common reed, Figure 4). This observation is
500 intriguing because a (bio)chemical process enriching heavy silicon isotopes has not been found to date.
501 Precipitation and adsorption of both abiogenic and biogenic silicon is known to enrich the light isotopes
502 in the precipitate (Oelze et al. 2014, Geilert et al. 2015, Frings et al. 2016). Thus, the solution remaining
503 after precipitation process will yield high δ^{30}Si. There are two possible pathways of such residual silicon

high in $\delta^{30}Si$ into phytoliths. Either the soil solutions' silicon available to the plants was previously depleted in light isotopes by, for example, neo-formation of secondary minerals, or these phytoliths formed from an intra-plant silicon pool that was depleted in the light isotope by previous precipitation of bio-silica within the plant.

Conclusions

We have established an analytical routine based on femtosecond laser ablation inductively coupled plasma mass spectrometry (fsLA-MC-ICP-MS) for *in situ* analysis of stable silicon isotope composition of phytoliths.

In terms of sample preparation, the lowest uncertainties associated with the $\delta^{30}Si$ results were achieved by mounting phytolith samples with clear nail lacquer onto a PMMA sample holder. The traditional approach, using epoxy resin for embedding, impaired the measurements by loss of phytolith material during polishing and thus to low and highly variable ion beams signals during laser ablation and data acquisition.

Good agreement between phytolith $\delta^{30}Si$ results obtained by bulk solution MC-ICP-MS analysis after total sample decomposition and silicon purification with *in situ* determined silicon isotope ratio by fsLA-MC-ICP-MS validates the analytical method described in this study.

In terms of uncertainty, bulk analysis resulted in at least two-fold better precision for $^{30/28}Si$ (typically 2SD on reference materials was better than 0.11 ‰) over that found for the means of *in situ* analyses (2SD typically better than 0.24). If differences were found between results from *in situ* analyses and those from bulk solution MC-ICP-MS, we identified the origin from sample heterogeneity combined with incomplete capture of a phytolith population in the analysis of single fragments. Phytolith samples extracted from the soil horizons were more amalgamated (i.e., homogenisation of the phytoliths' fragments) due to the preparation technique, leading to easier analyses, and also to isotopic homogenisation on the scale of fsLA-MC-ICP-MS.

In terms of advantages, fsLA-MC-ICP-MS is the better-suited method for screening and characterising heterogeneous phytolith populations. We found that certain investigated species (bushgrass, common reed, and horsetail) show large internal variations amounting to up to 2 ‰ in $\delta^{30}Si$ between different phytolith fragments. Capturing such heterogeneity thus potentially opens the possibility to investigate pathways of silicon of plants grown *in vivo*, after removal of only small parts of plant tissues. Furthermore, using phytoliths from geo-archives could enable the exploration of past silicon biogeochemical and climate cycles.

Supplementary information

All data used in this study are available online as an open access supplementary dataset at GFZ Data Services http://doi.org/10.5880/gfz.3.3.2018.002. (Frick et al. 2018)

Conflict of Interest

The authors have no conflict of interest to declare.

Acknowledgements

D.A.F. thanks the Swiss National Science Foundation for an Early Postdoc.Mobility fellowship (P2EZP2_168836), and the GFZ German Research Centre for Geosciences, the Helmholtz Laboratory for the Geochemistry of the Earth Surface (HELGES) and the Leibniz Centre for Agricultural Landscape Research for providing excellent (laboratory) infrastructure. The authors would like to thank Josefine Buhk and Jutta Schlegel for their support in HELGES, Danuta Kaczorek, ZALF, for the extraction of phytoliths and two anonymous reviewers for their helpful reviews that improved this manuscript.

References

Alexandre, A., Crespin, J., Sylvestre, F., Sonzogni, C., and Hilbert, D. W. (**2012**) The oxygen isotopic composition of phytolith assemblages from tropical rainforest soil tops (Queensland, Australia): validation of a new paleoenvironmental tool. **Climate of the Past**, **8**, 307–324.

Alexandre, A., Meunier, J.-D., Colin, F., and Koud, J.-M. (**1997**) Plant impact on the biogeochemical cycle of silicon and related weathering processes. **Geochimica et Cosmochimica Acta**, **61**, 677–682.

Allenby, R. J. (**1954**) Determination of the isotopic ratios of silicon in rocks. **Geochimica et Cosmochimica Acta**, **5**, 40–48.

Bern, C. R., Brzezinski, M. A., Beucher, C., Ziegler, K., and Chadwick, O. A. (**2010**) Weathering, dust, and biocycling effects on soil silicon isotope ratios. **Geochimica et Cosmochimica Acta**, **74**, 876–889.

von Blanckenburg, F., Wittmann, H., and Schuessler, J. A. (**2016**) HELGES: Helmholtz Laboratory for the Geochemistry of the Earth Surface. **Journal of large-scale research facilities JLSRF**, **2**, A84.

Bouchez, J., von Blanckenburg, F., and Schuessler, J. A. (**2013**) Modeling novel stable isotope ratios in the weathering zone. **American Journal of Science**, **313**, 267–308.

Coplen, T. B., Hopple, J. a, Böhlke, J. K., Peiser, H. S., Rieder, S. E., Krouse, H. R., Rosman, K. J. R., Ding, T., Vocke, R. D. J., Révész, K. M., Lamberty, A., Taylor, P., and Bièvre, P. De. (**2002**) Compilation of minimum and maximum isotope ratios of selected elements in naturally occurring

terrestrial materials and reagents. **U.S. Geological Survey Water-Resources Investigations Report 01-4222**, 45–50.

Cornelis, J.-T. T., Delvaux, B., Cardinal, D., André, L., Ranger, J., and Opfergelt, S. (**2010**) Tracing mechanisms controlling the release of dissolved silicon in forest soil solutions using Si isotopes and Ge/Si ratios. **Geochimica et Cosmochimica Acta**, **74**, 3913–3924.

Delvigne, C., Opfergelt, S., Cardinal, D., Delvaux, B., and André, L. (**2009**) Distinct silicon and germanium pathways in the soil-plant system: Evidence from banana and horsetail. **Journal of Geophysical Research: Biogeosciences**, **114**,.

Deshmukh, R. K., Ma, J. F., and Bélanger, R. R. (**2017**) Editorial: Role of Silicon in Plants. **Frontiers in Plant Science**, **8**, 1137–1145.

Ding, T. P., Ma, G. R., Shui, M. X., Wan, D. F., and Li, R. H. (**2005**) Silicon isotope study on rice plants from the Zhejiang province, China. **Chemical Geology**, **218**, 41–50.

Ding, T. P., Tian, S. H., Sun, L., Wu, L. H., Zhou, J. X., and Chen, Z. Y. (**2008a**) Silicon isotope fractionation between rice plants and nutrient solution and its significance to the study of the silicon cycle. **Geochimica et Cosmochimica Acta**, **72**, 5600–5615.

Ding, T. P., Zhou, J. X., Wan, D. F., Chen, Z. Y., Wang, C. Y., and Zhang, F. (**2008b**) Silicon isotope fractionation in bamboo and its significance to the biogeochemical cycle of silicon. **Geochimica et Cosmochimica Acta**, **72**, 1381–1395.

Douthitt, C. B. (**1982**) The geochemistry of the stable isotopes of silicon. **Geochimica et Cosmochimica Acta**, **46**, 1449–1458.

Ellison, S. L. R., and Williams, A., editors. (**2012**) Quantifying Uncertainty in Analytical Measurement. Page English.

Engström, E., Rodushkin, I., Öhlander, B., Ingri, J., and Baxter, D. C. (**2008**) Silicon isotopic composition of boreal forest vegetation in Northern Sweden. **Chemical Geology**, **257**, 247–256.

Epstein, E. (**1999**) Emanuel Epstein. **Annu. Rev.Plant Physiol. Plant Mol. Biol.**, 641–664.

Flamigni, L., Koch, J., and Günther, D. (**2012**) Experimental and theoretical investigations about the vaporization of laser-produced aerosols and individual particles inside inductively-coupled plasmas - Implications for the extraction efficiency of ions prior to mass spectrometry. **Spectrochimica Acta - Part B Atomic Spectroscopy**, **76**, 70–76.

Flamigni, L., Koch, J., and Günther, D. (**2014**) The effect of carrier gas humidity on the vaporization of laser-produced aerosols in inductively coupled plasmas. **J. Anal. At. Spectrom.**, **29**, 280–286.

Fliegel, D., Frei, C., Fontaine, G., Hu, Z. C., Gao, S., and Günther, D. (**2011**) Sensitivity improvement in laser ablation inductively coupled plasma mass spectrometry achieved using a methane/argon and methanol/water/argon mixed gas plasma. **Analyst**, **136**, 4925–4934.

Fraysse, F., Pokrovsky, O. S., and Meunier, J. D. (**2010**) Experimental study of terrestrial plant litter interaction with aqueous solutions. **Geochimica et Cosmochimica Acta**, **74**, 70–84.

Fraysse, F., Pokrovsky, O. S., Schott, J., and Meunier, J. D. (**2006**) Surface properties, solubility and dissolution kinetics of bamboo phytoliths. **Geochimica et Cosmochimica Acta**, **70**, 1939–1951.

Fraysse, F., Pokrovsky, O. S., Schott, J., and Meunier, J. D. (**2009**) Surface chemistry and reactivity of plant phytoliths in aqueous solutions. **Chemical Geology**, **258**, 197–206.

Frick, D. A., and Günther, D. (**2012**) Fundamental studies on the ablation behaviour of carbon in LA-ICP-MS with respect to the suitability as internal standard. **Journal of Analytical Atomic Spectrometry**, **27**, 1294.

Frick, D. A., Schuessler, J. A., and von Blanckenburg, F. (**2016**) Development of routines for simultaneous in situ chemical composition and stable Si isotope ratio analysis by femtosecond laser ablation inductively coupled plasma mass spectrometry. **Analytica Chimica Acta**, **938**, 33–43.

Frick, D. A., Schuessler, J. A., Sommer, M., and von Blanckenburg, F. (**2018**) Data supplement to: Laser ablation in situ silicon stable isotope analysis of phytoliths. **GFZ Data Services**,.

Frings, P. J., Clymans, W., Fontorbe, G., De La Rocha, C. L., and Conley, D. J. (**2016**) The continental Si cycle and its impact on the ocean Si isotope budget. **Chemical Geology**, **425**, 12–36.

Geilert, S., Vroon, P., Keller, N., Gudbrnadsson, S., and Stefánsson, A. (**2015**) Silicon isotope fractionation during silica precipitation from hot-spring waters. **Geochimica et Cosmochimica Acta**, **164**, 403–427.

Georg, R. B., Reynolds, B. C., Frank, M., and Halliday, A. N. (**2006**) New sample preparation techniques for the determination of Si isotopic compositions using MC-ICPMS. **Chemical Geology**, **235**, 95–104.

Haghighi, M., Afifipour, Z., and Mozafarian, M. (**2012**) The alleviation effect of silicon on seed germination and seedling growth of tomato under salinity stress. **Vegetable Crops Research Bulletin**, **76**, 119–126.

Hodson, M. J. (**2016**) The development of phytoliths in plants and its influence on their chemistry and isotopic composition. Implications for palaeoecology and archaeology. **Journal of Archaeological**

628 **Science**, **68**, 62–69.

629 **Hodson, M. J., Parker, A. G., Leng, M. J., and Sloane, H. J.** (**2008**) Silicon, oxygen and carbon isotope
630 composition of wheat (Triticum aestivum L.) phytoliths: implications for palaeoecology and
631 archaeology. **Journal of Quaternary Science**, **23**, 331–339.

632 **Janney, P. E., Richter, F. M., Mendybaev, R. A., Wadhwa, M., Georg, R. B., Watson, E. B., and Hines,**
633 **R. R.** (**2011**) Matrix effects in the analysis of Mg and Si isotope ratios in natural and synthetic
634 glasses by laser ablation-multicollector ICPMS: A comparison of single- and double-focusing mass
635 spectrometers. **Chemical Geology**, **281**, 26–40.

636 **JCGM**. (**2008**) JCGM 200 : 2008 International vocabulary of metrology — Basic and general concepts
637 and associated terms (VIM) Vocabulaire international de métrologie — Concepts fondamentaux
638 et généraux et termes associés (VIM). **International Organization for Standardization Geneva**
639 **ISBN**, **3**, 104.

640 **Jochum, K. P., Nohl, U., Herwig, K., Lammel, E., Stoll, B., and Hofmann, A. W.** (**2005**) GeoReM: A New
641 Geochemical Database for Reference Materials and Isotopic Standards. **Geostandards and**
642 **Geoanalytical Research**, **29**, 333–338.

643 **Jochum, K. P., Stoll, B., Weis, U., Jacob, D. E., Mertz-Kraus, R., and Andreae, M. O.** (**2014**) Non-Matrix-
644 Matched Calibration for the Multi-Element Analysis of Geological and Environmental Samples
645 Using 200 nm Femtosecond LA-ICP-MS: A Comparison with Nanosecond Lasers. **Geostandards**
646 **and Geoanalytical Research**, **38**, 265–292.

647 **Köster, J. R., Bol, R., Leng, M. J., Parker, A. G., Sloane, H. J., and Ma, J. F.** (**2009**) Effects of active silicon
648 uptake by rice on 29Si fractionation in various plant parts. **Rapid Communications in Mass**
649 **Spectrometry**, **23**, 2398–2402.

650 **De La Rocha, C. L.** (**2002**) Measurement of silicon stable isotope natural abundances via multicollector
651 inductively coupled plasma mass spectrometry (MC-ICP-MS). **Geochemistry Geophysics**
652 **Geosystems**, **3**, 1–8.

653 **De La Rocha, C. L., Brzezinski, M. A., and DeNiro, M. J.** (**1996**) Purification, Recovery, and Laser-Driven
654 Fluorination of Silicon from Dissolved and Particulate Silica for the Measurement of Natural
655 Stable Isotope Abundances. **Analytical Chemistry**, **68**, 3746–3750.

656 **Ma, J. F., Tamai, K., Yamaji, N., Mitani, N., Konishi, S., Katsuhara, M., Ishiguro, M., Murata, Y., and**
657 **Yano, M.** (**2006**) A silicon transporter in rice. **Nature**, **440**, 688–691.

658 **Ma, J. F., and Yamaji, N.** (**2015**) A cooperative system of silicon transport in plants. **Trends in Plant**

659 **Science**, **20**, 435–442.

660 **Ma, J. F., Yamaji, N., and Mitani-Ueno, N.** (**2011**) Transport of silicon from roots to panicles in plants.
661 **Proceedings of the Japan Academy. Series B, Physical and biological sciences**, **87**, 377–385.

662 **Marschner, H., and Marschner, P.** (**2012**) Marschner's mineral nutrition of higher plants. Academic
663 Press.

664 **Oelze, M., von Blanckenburg, F., Hoellen, D., Dietzel, M., and Bouchez, J.** (**2014**) Si stable isotope
665 fractionation during adsorption and the competition between kinetic and equilibrium isotope
666 fractionation: Implications for weathering systems. **Chemical Geology**, **380**, 161–171.

667 **Oelze, M., Schuessler, J. A., and von Blanckenburg, F.** (**2016**) Mass bias stabilization by Mg doping for
668 Si stable isotope analysis by MC-ICP-MS. **J. Anal. At. Spectrom.**, **31**, 2094–2100.

669 **Opfergelt, S., Cardinal, D., André, L., Delvigne, C., Bremond, L., and Delvaux, B.** (**2010**) Variations of
670 δ30Si and Ge/Si with weathering and biogenic input in tropical basaltic ash soils under
671 monoculture. **Geochimica et Cosmochimica Acta**, **74**, 225–240.

672 **Opfergelt, S., Cardinal, D., Henriet, C., Draye, X., André, L., and Delvaux, B.** (**2006**) Silicon Isotopic
673 Fractionation by Banana (Musa spp.) Grown in a Continuous Nutrient Flow Device. **Plant and Soil**,
674 **285**, 333–345.

675 **Opfergelt, S., and Delmelle, P.** (**2012**) Silicon isotopes and continental weathering processes: Assessing
676 controls on Si transfer to the ocean. **Comptes Rendus - Geoscience**, **344**, 723–738.

677 **Opfergelt, S., Delvaux, B., André, L., and Cardinal, D.** (**2008**) Plant silicon isotopic signature might
678 reflect soil weathering degree. **Biogeochemistry**, **91**, 163–175.

679 **Piperno, D. R.** (**2006**) Phytoliths : a comprehensive guide for archaeologists and paleoecologists.
680 AltaMira Press, Lanham, MD.

681 **Prentice, A. J., and Webb, E. A.** (**2016**) The effect of progressive dissolution on the oxygen and silicon
682 isotope composition of opal-A phytoliths: Implications for palaeoenvironmental reconstruction.
683 **Palaeogeography, Palaeoclimatology, Palaeoecology**, **453**, 42–51.

684 **Puppe, D., Höhn, A., Kaczorek, D., Wanner, M., Wehrhan, M., and Sommer, M.** (**2017**) How big is the
685 influence of biogenic silicon pools on short-term changes in water-soluble silicon in soils?
686 Implications from a study of a 10-year-old soil-plant system. **Biogeosciences**, **14**, 5239–5252.

687 **Rios, J. J., Martínez-Ballesta, M. C., Ruiz, J. M., Blasco, B., and Carvajal, M.** (**2017**) Silicon-mediated
688 Improvement in Plant Salinity Tolerance: The Role of Aquaporins. **Frontiers in Plant Science**, **8**,
689 1–10.

Riotte, J., Meunier, J. D., Zambardi, T., Audry, S., Barboni, D., Anupama, K., Prasad, S., Chmeleff, J., Poitrasson, F., Sekhar, M., and Braun, J. J. (**2018**) Processes controlling silicon isotopic fractionation in a forested tropical watershed: Mule Hole Critical Zone Observatory (Southern India). **Geochimica et Cosmochimica Acta**, **228**, 301–319.

Rodrigues, F. A., and Datnoff, L. E. (**2015**) Silicon and plant diseases. Page Silicon and Plant Diseases.

Schuessler, J. A., and von Blanckenburg, F. (**2014**) Testing the limits of micro-scale analyses of Si stable isotopes by femtosecond laser ablation multicollector inductively coupled plasma mass spectrometry with application to rock weathering. **Spectrochimica Acta Part B: Atomic Spectroscopy**, **98**, 1–18.

Sommer, M., Jochheim, H., Höhn, A., Breuer, J., Zagorski, Z., Busse, J., Barkusky, D., Meier, K., Puppe, D., Wanner, M., and Kaczorek, D. (**2013**) Si cycling in a forest biogeosystem - the importance of transient state biogenic Si pools. **Biogeosciences**, **10**, 4991–5007.

Sommer, M., Kaczorek, D., Kuzyakov, Y., and Breuer, J. (**2006**) Silicon pools and fluxes in soils and landscapes—a review. **Journal of Plant Nutrition and Soil Science**, **169**, 310–329.

Steinhoefel, G., Breuer, J., von Blanckenburg, F., Horn, I., Kaczorek, D., and Sommer, M. (**2011**) Micrometer silicon isotope diagnostics of soils by UV femtosecond laser ablation. **Chemical Geology**, **286**, 280–289.

Steinhoefel, G., Breuer, J., von Blanckenburg, F., Horn, I., and Sommer, M. (**2017**) The dynamics of Si cycling during weathering in two small catchments in the Black Forest (Germany) traced by Si isotopes. **Chemical Geology**, **466**, 389–402.

Sun, L., Wu, L. H., Ding, T. P., and Tian, S. H. (**2008**) Silicon isotope fractionation in rice plants, an experimental study on rice growth under hydroponic conditions. **Plant and Soil**, **304**, 291–300.

Sun, Y., Wu, L., and Li, X. (**2016a**) Experimental Determination of Silicon Isotope Fractionation in Rice. **PLOS ONE**, **11**, e0168970.

Sun, Y., Wu, L., Li, X., Sun, L., Gao, J., and Ding, T. (**2016b**) Silicon Isotope Fractionation in Rice and Cucumber Plants over a Life Cycle: Laboratory Studies at Different External Silicon Concentrations. **Journal of Geophysical Research: Biogeosciences**, 2829–2841.

Sutton, J. N., André, L., Cardinal, D., Conley, D. J., de Souza, G. F., Dean, J., Dodd, J., Ehlert, C., Ellwood, M. J., Frings, P. J., Grasse, P., Hendry, K., Leng, M. J., Michalopoulos, P., Panizzo, V. N., and Swann, G. E. A. (**2018**) A Review of the Stable Isotope Bio-geochemistry of the Global Silicon Cycle and Its Associated Trace Elements. **Frontiers in Earth Science**, **5**,.

721 **Tatzel, M., von Blanckenburg, F., Oelze, M., Schuessler, J. A., and Bohrmann, G.** (**2015**) The silicon
722 isotope record of early silica diagenesis. **Earth and Planetary Science Letters**, **428**, 293–303.

723 **Watteau, F., and Villemin, G.** (**2001**) Ultrastructural study of the biogeochemical cycle of silicon in the
724 soil and litter of a temperate forest. **European Journal of Soil Science**, **52**, 385–396.

725 **Zambardi, T., and Poitrasson, F.** (**2011**) Precise Determination of Silicon Isotopes in Silicate Rock
726 Reference Materials by MC-ICP-MS. **Geostandards and Geoanalytical Research**, **35**, 89–99.

727 **Zheng, X.-Y., Beard, B. L., and Johnson, C. M.** (**2018**) Assessment of matrix effects associated with Fe
728 isotope analysis using 266 nm femtosecond and 193 nm nanosecond laser ablation multi-
729 collector inductively coupled plasma mass spectrometry. **Journal of Analytical Atomic**
730 **Spectrometry**, **33**, 68–83.

731 **Ziegler, K., Chadwick, O. A., Brzezinski, M. A., and Kelly, E. F.** (**2005**) Natural variations of δ30Si ratios
732 during progressive basalt weathering, Hawaiian Islands. **Geochimica et Cosmochimica Acta**, **69**,
733 4597–4610.

734

List of Figures

List of Tables

Supplement to "Laser ablation *in situ* silicon stable isotope analysis of phytoliths"

Daniel A. Frick[1, ‡], Jan A. Schuessler[1], Michael Sommer[2,3], Friedhelm von Blanckenburg[1,4]

[1] GFZ German Research Centre for Geosciences, Earth Surface Geochemistry, Potsdam, Germany.

[2] Leibniz-Centre for Agricultural Landscape Research (ZALF) e. V., Working Group Si Biogeochemistry, 15374 Müncheberg, Germany.

[3] University of Potsdam, Institute of Earth and Environmental Sciences, Karl-Liebknecht-Str. 24-24, 14476 Potsdam, Germany.

[4] Institute of Geological Science, Freie Universität Berlin, Berlin.

+4933128828963

Content

Table S1: Instrument configuration of Faraday cup and amplifier settings for bulk solution MC-ICP-MS Si isotope measurements. There is a 3 s delay time between line 1 and line 2.

Faraday Cup	**L3**	**L2**	**L1**	**C**	**H2**
Line 1	^{28}Si		^{29}Si	^{30}Si	
Line 2		^{24}Mg		^{25}Mg	^{26}Mg
Amplifier	10^{11} Ω	10^{11} Ω	10^{11} Ω	10^{11} Ω	10^{11} Ω

*Table S2: Instrument settings for bulk solution MC-ICP-MS Si isotope measurements. *Parameters tuned for best sensitivity, stability and peak shape before each measurement session.*

Cool Gas Flow	15.00	[L min^{-1}]	Extraction Lens	-2000	[V]
Auxiliary Gas Flow	0.80	[L min^{-1}]	Focus Lens*	-651	[V]
Nebuliser Gas Flow	1.071*	[L min^{-1}]	X-Deflection*	-2.87	[V]
RF Power	1200	[W]	Y-Deflection*	-2.97	[V]
Torch:			Shape*	202	[V]
X*	1.010	[mm]	Rotation Quad 1*	2.03	[V]
Y*	-3.760	[mm]	Source Offset	0.0	[V]
Z*	-1.250	[mm]	Focus Quad 1*	-19.89	[V]
Sampler Cone	Ni Jet		Rotation Quad* 2	0	[V]
Skimmer Cone	Ni H		Focus Offset*	50.00	[V]
Focus Quad*	-1.0	[V]	Matsuda Plate	0.0	[V]
Dispersion	0.0	[V]			
Apex: Heat: 2, Cool: 2 with PFA nebuliser with 160µL/min measured uptake rate.					
Cycles	30		Integration time	4.194	[s/cycle]

Table S3: Instrument configuration of Faraday cup and amplifier settings for fsLA MC-ICP-MS Si isotope analysis.

Faraday Cup	**L4**	**L2**	**C**	**H2**
Line 1	^{27}Al	^{28}Si	^{29}Si	^{30}Si
Amplifier	10^{11} Ω	10^{11} Ω	10^{11} Ω	10^{11} Ω

*Table S4: Typical laser settings used throughout the study. *Laser repetition rate was adjusted to attain uniform 28Si ion beam intensities during measurements (matched to bracketing standard signal intensity).*

Crater size	25-30	[µm]
Repetition rate*	15-125	[Hz]
Scan velocity	40	[µm/s]
Energy density	1.2-1.5	J/cm²
Wavelength	196	[nm]

*Table S5 Instrument settings used for in situ fsLA fsLA MC-ICP-MS Si isotope analysis. *Parameters tuned for best sensitivity, stability and peak shape before each measurement session. Auxiliary and nebuliser gas flows were within 0.1 L min^{-1} for the different measurement sessions.*

Cool Gas Flow	15.00	[L min^{-1}]	Extraction Lens	-2000	[V]
Auxiliary Gas Flow*	0.6	[L min^{-1}]	Focus Lens*	-582	[V]
Nebuliser Gas Flow*	0.6	[L min^{-1}]	X-Deflection*	-4.06	[V]
Helium Gas Flow*	1.1	[L min^{-1}]	Y-Deflection*	-2.24	[V]
RF Power	1250	[W]	Shape*	204	[V]
Torch:			Rotation Quad 1*	2.91	[V]
X*	1.090	[mm]	Source Offset	-1.0	[V]
Y*	-3.670	[mm]	Focus Quad 1*	-19.89	[V]
Z*	-0.900	[mm]	Rotation Quad 2*	0.0	[V]
Sampler Cone	Ni	Jet	Focus Offset	50.00	[V]
Skimmer Cone	Ni	H	Matsuda Plate	0.0	[V]
Focus Quad*	-2.10	[V]			
Dispersion	0.0	[V]			
PFA Nebuliser with a measured uptake rate of 50 µL/min					
Cycles	200		Integration time	1.049	[s/cycle]

Table S6: Silicon isotope ratio results from solution MC-ICP-MS analysis (after alkali fusion and Si purification) of international reference materials. Mean δ-values with their 2 standard deviations (2SD) of n repeat MC-ICP-MS analysis are reported relative to NBS28.

	Bulk solution MC-ICP-MS results (this study)					**Averages of published values***			
	$\delta^{29}Si/^{28}Si_{NBS28}$ (‰)	**2SD**	**$\delta^{30}Si/^{28}Si_{NBS28}$ (‰)**	**2SD**	**n**	**$\delta^{29}Si/^{28}Si_{NBS28}$ (‰)**	**2SD**	**$\delta^{30}Si/^{28}Si_{NBS28}$ (‰)**	**2SD**
BHVO-2	-0.11	0.05	-0.24	0.01	4	-0.14	0.05	-0.28	0.09
ERM-CD281	-0.15	0.06	-0.28	0.08	3	-	-	-	-

**Values for BHVO-2 from* (Jochum et al. 2005) *and* (van den Boorn et al. 2006, Abraham et al. 2008, Fitoussi et al. 2009, Savage et al. 2010, 2011, 2012, 2013a, 2013b, Opfergelt et al. 2011, 2012, Zambardi and Poitrasson 2011, Armytage et al. 2011, 2012, Pogge von Strandmann et al. 2012, Pringle et al. 2013, 2016, Savage and Moynier 2013, Kempl et al. 2013, Geilert et al. 2014a, 2014b, 2015, Dauphas et al. 2015, Tatzel et al. 2015, Mavromatis et al. 2016, Reddy et al. 2016, Zheng et al. 2016, Chen et al. 2017)

Table S7: Silicon isotope ratio results from in situ fsLA MC-ICP-MS analysis of international reference materials. Mean δ-values with their 2 standard deviations (2SD) of n repeat fsLA MC-ICP-MS analysis are reported relative to NIST SRM610.

	***In situ* fsLA MC-ICP-MS results**					**Averages of published values***			
	$\delta^{29}Si/^{28}Si_{NIST610}$ (‰)	**2SD**	**$\delta^{30}Si/^{28}Si_{NIST610}$ (‰)**	**2SD**	**n**	**$\delta^{29}Si/^{28}Si_{NBS28}$ (‰)**	**2SD**	**$\delta^{30}Si/^{28}Si_{NBS28}$ (‰)**	**2SD**
ATHO-G	-0.13	0.18	-0.25	0.24	24	-0.19	0.12	-0.39	0.29
BHVO-2	-0.18	0.13	-0.32	0.20	46	-0.14	0.05	-0.28	0.09
GOR132-G	-0.17	0.14	-0.36	0.18	10	-0.15	0.12	-0.27	0.21
NBS28	-0.02	0.15	-0.08	0.14	6	≡ 0	-	≡ 0	-
NIST612	-0.01	0.12	0.01	0.13	16	-0.02	0.07	-0.02	0.11

**for ATHO-G:* (Jochum et al. 2011, Schuessler and von Blanckenburg 2014, Frick et al. 2016)*, for BHVO-2* (van den Boorn et al. 2006, Abraham et al. 2008, Fitoussi et al. 2009, Savage et al. 2010, 2011, 2012, 2013a, 2013b, Opfergelt et al. 2011, 2012, Zambardi and Poitrasson 2011, Armytage et al. 2011, 2012, Pogge von Strandmann et al. 2012, Pringle et al. 2013, 2016, Savage and Moynier 2013, Kempl et al. 2013, Geilert et al. 2014a, 2014b, 2015, Dauphas et al. 2015, Tatzel et al. 2015, Mavromatis et al. 2016, Reddy et al. 2016, Zheng et al. 2016, Chen et al. 2017)*, for GOR132-G* (Jochum et al. 2011) *and NIST612* (Schuessler and von Blanckenburg 2014, Frick et al. 2016)

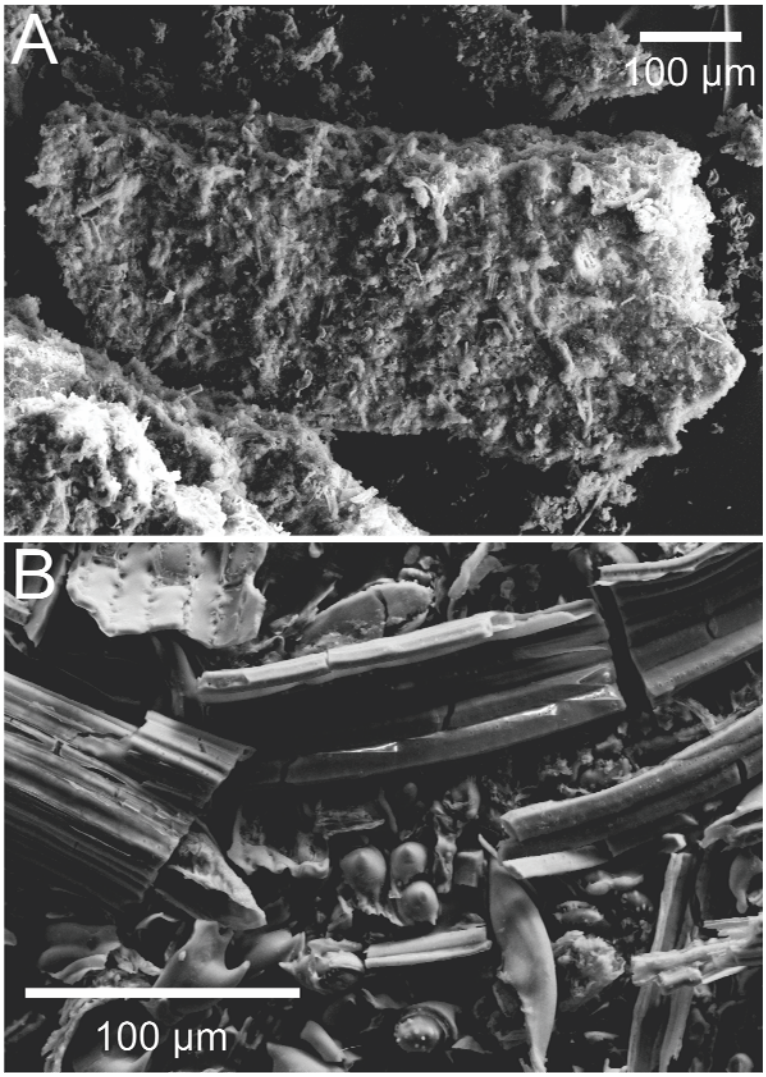

S-Figure 1: SEM image details of European beech (A) and Norway spruce (B). Both samples consist of finely-ground phytoliths material, indicating a homogenisation process has taken place during the decomposition in the soil or the sample preparation steps. Close inspection of the European beech phytolith fragments reveal a compacted structure of finely-ground fragments. Scale bar are 100 µm.

Literature

Abraham, K., Opfergelt, S., Fripiat, F., Cavagna, a-J., de Jong, J. T. M., Foley, S., Andre, L., and Cardinal, D. (**2008**) d30Si and d29Si determination on BHVO-1 and BHVO-2 reference materials with a new configuration on a Nu Plasma Multi Collector ICP-MS. **Geostandards and Geoanalytical Research**, **32**, 193–202.

Armytage, R. M. G., Georg, R. B., Savage, P. S., Williams, H. M., and Halliday, A. N. (**2011**) Silicon isotopes in meteorites and planetary core formation. **Geochimica et Cosmochimica Acta**, **75**, 3662–3676.

Armytage, R. M. G., Georg, R. B., Williams, H. M., and Halliday, A. N. (**2012**) Silicon isotopes in lunar rocks: Implications for the Moon's formation and the early history of the Earth. **Geochimica et Cosmochimica Acta**, **77**, 504–514.

van den Boorn, S. H. J. M., Vroon, P. Z., van Belle, C. C., van der Wagt, B., Schwieters, J., and van Bergen, M. J. (**2006**) Determination of silicon isotope ratios in silicate materials by high-resolution MC-ICP-MS using a sodium hydroxide sample digestion method. **Journal of Analytical Atomic Spectrometry**, **21**, 734.

Chen, X., Lapen, T. J., and Chafetz, H. S. (**2017**) Accurate and Precise Silicon Isotope Analysis of Sulfur- and Iron-Rich Samples by MC-ICP-MS. **Geostandards and Geoanalytical Research**, **41**, 427–435.

Dauphas, N., Poitrasson, F., Burkhardt, C., Kobayashi, H., and Kurosawa, K. (**2015**) Planetary and meteoritic Mg/Si and δ^{30}Si variations inherited from solar nebula chemistry. **Earth and Planetary Science Letters**, **427**, 236–248.

Fitoussi, C., Bourdon, B., Kleine, T., Oberli, F., and Reynolds, B. C. (**2009**) Si isotope systematics of meteorites and terrestrial peridotites: implications for Mg/Si fractionation in the solar nebula and for Si in the Earth's core. **Earth and Planetary Science Letters**, **287**, 77–85.

Frick, D. A., Schuessler, J. A., and von Blanckenburg, F. (**2016**) Development of routines for simultaneous in situ chemical composition and stable Si isotope ratios analyses by femtosecond laser ablation inductively coupled plasma mass spectrometry. **Analytica Chimica Acta**, **938**, 33–43.

Geilert, S., Vroon, P. Z., and van Bergen, M. J. (**2014a**) Silicon isotopes and trace elements in chert record early Archean basin evolution. **Chemical Geology**, **386**, 133–142.

Geilert, S., Vroon, P. Z., Keller, N. S., Gudbrandsson, S., Stefánsson, A., and van Bergen, M. J. (**2015**) Silicon isotope fractionation during silica precipitation from hot-spring waters: Evidence from the Geysir geothermal field, Iceland. **Geochimica et Cosmochimica Acta**, **164**, 403–427.

Geilert, S., Vroon, P. Z., Roerdink, D. L., Van Cappellen, P., and van Bergen, M. J. (**2014b**) Silicon isotope fractionation during abiotic silica precipitation at low temperatures: Inferences from flow-through experiments. **Geochimica et Cosmochimica Acta**, **142**, 95–114.

Jochum, K. P., Nohl, U., Herwig, K., Lammel, E., Stoll, B., and Hofmann, A. W. (**2005**) GeoReM: A New Geochemical Database for Reference Materials and Isotopic Standards. **Geostandards and Geoanalytical Research**, **29**, 333–338.

Jochum, K. P., Wilson, S. A., Abouchami, W., Amini, M., Chmeleff, J., Eisenhauer, A., Hegner, E., Iaccheri, L. M., Kieffer, B., Krause, J., Mcdonough, W. F., Mertz-Kraus, R., Raczek, I., Rudnick, R. L., Scholz, D., Steinhoefel, G., Stoll, B., Stracke, A., Tonarini, S., Weis, D., Weis, U., and Woodhead, J. D. (**2011**) GSD-1G and MPI-DING Reference Glasses for In Situ and Bulk Isotopic Determination. **Geostandards and Geoanalytical Research**, **35**, 193–226.

Kempl, J., Vroon, P. Z., Zinngrebe, E., and van Westrenen, W. (**2013**) Si isotope fractionation between Si-poor metal and silicate melt at pressure-temperature conditions relevant to metal segregation in small planetary bodies. **Earth and Planetary Science Letters**, **368**, 61–68.

Mavromatis, V., Rinder, T., Prokushkin, A. S., Pokrovsky, O. S., Korets, M. A., Chmeleff, J., and Oelkers, E. H.

(**2016**) The effect of permafrost, vegetation, and lithology on Mg and Si isotope composition of the Yenisey River and its tributaries at the end of the spring flood. **Geochimica et Cosmochimica Acta**, **191**, 32–46.

Opfergelt, S., Eiriksdottir, E. S., Burton, K. W., Einarsson, A., Siebert, C., Gislason, S. R., and Halliday, A. N. (**2011**) Quantifying the impact of freshwater diatom productivity on silicon isotopes and silicon fluxes: Lake Myvatn, Iceland. **Earth and Planetary Science Letters**, **305**, 73–82.

Opfergelt, S., Georg, R. B. B., Delvaux, B., Cabidoche, Y.-M. M., Burton, K. W. W., and Halliday, A. N. N. (**2012**) Silicon isotopes and the tracing of desilication in volcanic soil weathering sequences, Guadeloupe. **Chemical Geology**, **326–327**, 113–122.

Pogge von Strandmann, P. A. E., Opfergelt, S., Lai, Y.-J., Sigfússon, B., Gislason, S. R., and Burton, K. W. (**2012**) Lithium, magnesium and silicon isotope behaviour accompanying weathering in a basaltic soil and pore water profile in Iceland. **Earth and Planetary Science Letters**, **339–340**, 11–23.

Pringle, E. A., Moynier, F., Savage, P. S., Jackson, M. G., Moreira, M., and Day, J. M. D. (**2016**) Silicon isotopes reveal recycled altered oceanic crust in the mantle sources of Ocean Island Basalts. **Geochimica et Cosmochimica Acta**, **189**, 282–295.

Pringle, E. A., Savage, P. S., Badro, J., Barrat, J. A., and Moynier, F. (**2013**) Redox state during core formation on asteroid 4-Vesta. **Earth and Planetary Science Letters**, **373**, 75–82.

Reddy, T. R., Zheng, X.-Y. Y., Roden, E. E., Beard, B. L., and Johnson, C. M. (**2016**) Silicon isotope fractionation during microbial reduction of Fe(III)-Si gels under Archean seawater conditions and implications for iron formation genesis. **Geochimica et Cosmochimica Acta**, **190**, 85–99.

Savage, P. S., Georg, R. ., Armytage, R. M. G., Williams, H. M., and Halliday, A. N. (**2010**) Silicon isotope homogeneity in the mantle. **Earth and Planetary Science Letters**, **295**, 139–146.

Savage, P. S., Georg, R. B., Williams, H. M., Burton, K. W., and Halliday, A. N. (**2011**) Silicon isotope fractionation during magmatic differentiation. **Geochimica et Cosmochimica Acta**, **75**, 6124–6139.

Savage, P. S., Georg, R. B., Williams, H. M., and Halliday, A. N. (**2013a**) The silicon isotope composition of the upper continental crust. **Geochimica et Cosmochimica Acta**, **109**, 384–399.

Savage, P. S., Georg, R. B., Williams, H. M., and Halliday, A. N. (**2013b**) Silicon isotopes in granulite xenoliths: Insights into isotopic fractionation during igneous processes and the composition of the deep continental crust. **Earth and Planetary Science Letters**, **365**, 221–231.

Savage, P. S., Georg, R. B., Williams, H. M., Turner, S., Halliday, A. N., and Chappell, B. W. (**2012**) The silicon isotope composition of granites. **Geochimica et Cosmochimica Acta**, **92**, 184–202.

Savage, P. S., and Moynier, F. (**2013**) Silicon isotopic variation in enstatite meteorites: Clues to their origin and Earth-forming material. **Earth and Planetary Science Letters**, **361**, 487–496.

Schuessler, J. A., and von Blanckenburg, F. (**2014**) Testing the limits of micro-scale analyses of Si stable isotopes

by femtosecond laser ablation multicollector inductively coupled plasma mass spectrometry with application to rock weathering. **Spectrochimica Acta Part B: Atomic Spectroscopy**, **98**, 1–18.

Tatzel, M., von Blanckenburg, F., Oelze, M., Schuessler, J. A., and Bohrmann, G. (**2015**) The silicon isotope record of early silica diagenesis. **Earth and Planetary Science Letters**, **428**, 293–303.

Zambardi, T., and Poitrasson, F. (**2011**) Precise Determination of Silicon Isotopes in Silicate Rock Reference Materials by MC-ICP-MS. **Geostandards and Geoanalytical Research**, **35**, 89–99.

Zheng, X.-Y., Beard, B. L., Reddy, T. R., Roden, E. E., and Johnson, C. M. (**2016**) Abiologic silicon isotope fractionation between aqueous Si and Fe(III)–Si gel in simulated Archean seawater: Implications for Si isotope records in Precambrian sedimentary rocks. **Geochimica et Cosmochimica Acta**, **187**, 102–122.